Two-Photon Fluorescence Spectroscopy and Microscopy of NAD(P)H and Flavoprotein

Shaohui Huang, Ahmed A. Heikal, and Watt W. Webb
School of Applied and Engineering Physics, Cornell University, Ithaca, New York 14853 USA

ABSTRACT Two-photon (2P) ratiometric redox fluorometry and microscopy of pyridine nucleotide (NAD(P)H) and flavoprotein (FP) fluorescence, at 800-nm excitation, has been demonstrated as a function of mitochondrial metabolic states in isolated adult dog cardiomyocytes. We have measured the 2P-excitation spectra of NAD(P)H, flavin adenine dinucleotide (FAD), and lipoamide dehydrogenase (LipDH) over the wavelength range of 720-1000 nm. The 2P-excitation action cross sections (σ_{2P}) increase rapidly at wavelengths below 800 nm, and the maximum σ_{2P} of LipDH is ~5 and 12 times larger than those of FAD and NAD(P)H, respectively. Only FAD and LipDH can be efficiently excited at wavelengths above 800 nm with a broad 2P-excitation band around 900 nm. Two autofluorescence spectral regions (i.e., ~410–490 nm and ~510–650 nm) of isolated cardiomyocytes were imaged using 2P-laser scanning microscopy. At 750-nm excitation, fluorescence of both regions is dominated by NAD(P)H emission, as indicated by fluorescence intensity changes induced by mitochondrial inhibitor NaCN and mitochondria uncoupler carbonyl cyanide *p*-(trifluoromethoxy) phenyl hydrazone (FCCP). In contrast, 2P-FP fluorescence dominates at 900-nm excitation, which is in agreement with the σ_{2P} measurements. Finally, 2P-autofluorescence emission spectra of single cardiac cells have been obtained, with results suggesting potential for substantial improvement of the proposed 2P-ratiometric technique.

INTRODUCTION

Redox fluorometry based on intrinsic fluorescence of reduced pyridine nucleotides (NADH and NADPH; hereafter NAD(P)H) and oxidized flavoproteins (FPs) has been a useful tool for studying cellular energy metabolism (reviewed by Balaban and Mandel, 1990; Chance, 1991; Masters, 1984; Masters and Chance, 1993). Previously, such methods involved one-photon (1P) excitation at near-UV and visible wavelengths for NAD(P)H and FP fluorescence, respectively. However, in situ applications of the 1P-redox fluorometry have been limited due to photobleaching of intrinsic fluorophores, photodamage to biological samples, and significant light scattering and absorption in turbid cell and tissue environments. These difficulties can be mostly overcome by using multiphoton microscopy (MPM) coupled with near-infrared (NIR) excitation. MPM provides advantages such as intrinsic three-dimensional resolution, negligible out-of-focus photobleaching, reduced light scattering and photodamage, and improved fluorescence collection efficiency (Denk et al., 1990; reviewed by Denk et al., 1995; Xu and Webb, 1997). Consequently, two-photon (2P) NAD(P)H fluorescence has been characterized and applied to several biological studies (Piston et al., 1995; Kierdaszuk et al., 1996; Konig et al., 1996; Masters et al., 1998; Piston et al., 1999; Patterson et al., 2000; Kasischke et al., 2001). However, little is known about the 2P characteristics of cellular FP fluorescence, despite its well-documented molecular origins.

Cellular flavins and flavin adenine dinucleotides (FADs) and mononucleotides (FMNs) exist mostly as cofactors for enzymes involved in oxidation-reduction reactions. There are dozens of such enzymes that are mostly non- or weakly fluorescent, because the fluorescence of their flavin cofactors is usually significantly quenched by the protein environment (Kunz and Kunz, 1985; Voltti and Hassinen, 1978). Early research has established that only lipoamide dehydrogenase (LipDH) and electron transfer flavoprotein (ETF) in mitochondrial matrix contribute significantly to cellular FP fluorescence (Hassinen and Chance, 1968; Hall and Kamin, 1975; Voltti and Hassinen, 1978; Kunz and Kunz, 1985; Kunz, 1986). By one estimate, LipDH constitutes ~50% of the FP fluorescence in rat liver mitochondria, ETF ~25%, and unspecific flavins the rest (Kunz and Kunz, 1985). LipDH is found in several 2-oxo acid dehydrogenase multienzyme complexes (reviewed by Perham, 1991), and the redox state of its FAD cofactor is in direct equilibrium with the mitochondrial NAD^+/NADH pool (i.e., NAD linked), as indicated by the simplified reaction mechanism below:

$$\mathrm{LipDH(FADH_2)} + \mathrm{NAD^+} \leftrightarrow \mathrm{LipDH(FAD)} + \mathrm{NADH} + \mathrm{H^+}$$

Similarly, ETF is involved in transferring the reducing equivalents resulting from β-oxidation of fatty acids to coenzyme-Q in the respiratory chain (i.e., CoQ linked), and its redox state is indirectly influenced by the mitochondrial NAD^+/NADH ratio (Hall and Kamin, 1975; Kunz and Kunz, 1985; Kunz, 1988). The rest of the FP signal is reducible only in the presence of dithionite (i.e., DIT reduc-

Submitted November 29, 2001, and accepted for publication January 3, 2002.

Address reprint requests to Dr. Watt W. Webb, School of Applied and Engineering Physics, 212 Clark Hall, Cornell University, Ithaca, NY 14853. Tel.: 607-255-3331; Fax: 607-255-7658; E-mail: www2@cornell.edu.

0006-3495/02/05/2811/15 $2.00

ible), and it is likely related to weakly fluorescent FPs and/or FPs that are not in redox contact with the respiratory chain (Kunz and Kunz, 1985; Kunz, 1986, 1988).

Because only oxidized FPs and reduced NAD(P)H are significantly fluorescent, these two signals respond oppositely to changes in mitochondrial metabolic states (Hassinen and Chance, 1968; Scholz et al., 1969; Kunz and Kunz, 1985; reviewed by Masters, 1984; Koenig and Schneckenburger, 1994). Consequently, ratiometric redox fluorometry based on NAD(P)H and FP fluorescence has been used to monitor cell and tissue metabolism, which minimizes interfering factors such as absorption of excitation and emission light by intrinsic chromophores (e.g., hemoglobin, myoglobin, and cytochromes), light scattering in turbid biological samples, and variations in mitochondrial density and FP concentrations (Scholz et al., 1969; Chance et al., 1979; Nuutinen et al., 1981; Kunz et al., 1994; Kuznetsov et al., 1998; Shiino et al., 1999). Previously, such ratiometric methods required two-color 1P excitation and time-sharing devices for alternate excitation and detection of the NAD(P)H and FP fluorescence (Quistorff et al., 1985; Masters, 1984). In contrast, both NAD(P)H and FPs can be simultaneously 2P excited at one NIR wavelength (Xu and Webb, 1997). Therefore, 2P-ratiometric redox fluorometry combines the advantages of MPM with the simplicity of one excitation light. Furthermore, with increasing in vivo applications of 2P-NAD(P)H fluorescence to studies of cell and tissue bioenergetics (Piston et al., 1995, 1999; Masters et al., 1998; Patterson et al., 2000; Kasischke et al., 2001), it is important to quantify the FP fluorescence contribution at wavelengths typically used for 2P-NAD(P)H excitation. Finally, compared with the NAD(P)H signal, FP fluorescence can be excited at longer excitation wavelengths, is much more resistant to photobleaching, and is almost exclusively associated with mitochondria (Scholz et al., 1969; Koke et al., 1981). Therefore, identifying conditions where 2P-FP fluorescence can be isolated will be useful for studies of mitochondrial functions and diseases (Berger et al., 1996; Kunz et al., 1997; Romashko et al., 1998; reviewed by Schoffner, 1997; Green and Reed, 1998; Wallace, 1999).

In this study, 2P-excitation action cross sections of NAD(P)H, FAD, and LipDH were first determined in solution over the wavelength range of 720-1000 nm typically used in MPM. These in vitro results guided subsequent imaging of 2P-NAD(P)H, FP, or both types of fluorescence in isolated adult dog cardiomyocytes. Further confirmation of the assignment of the cellular fluorescence to FP or NAD(P)H was provided by 2P-autofluorescence emission spectra of single cardiac cells.

MATERIALS AND METHODS

Materials

Sodium pentobarbital was purchased from Vertech Pharmaceuticals (Dearborn, MI). Collagenase (type II) was obtained from Worthington Biochemical (Lakewood, NJ). Bovine serum albumin (BSA), NaCN, carbonyl cyanide *p*-(trifluoromethoxy) phenyl hydrazone (FCCP), NADH, NADPH, FAD, and 2,4-dinitrophenol were purchased from Sigma (St. Louis, MO). Fluorescein was purchased from Molecular Probes (Eugene, OR). LipDH of bovine heart in 3.2 M $(NH_4)_2SO_4$ (pH 6.0) was purchased from Sigma. For the σ_{2P} measurements, the stock LipDH sample was desalted and exchanged into a new buffer containing 100 mM potassium phosphate (pH 7.6) and 20 mM EDTA using a Bio-Gel P6 spin column purchased from Pierce (Rockford, IL). Purity of the desalted LipDH was then checked by its absorption ratio at 273 and 455 nm. A ratio close to 5.3 was found, indicating a 1:1 stoichiometry of the oxidized cofactor FAD to LipDH (Patel et al., 1995). Other salts used in this study were purchased either from Sigma or Fisher Chemical (Pittsburgh, PA).

Epicardial myocyte preparation

Adult dog cardiomyocytes were isolated according to the protocol by Pacioretty and Gilmour (1998). Briefly, an adult beagle dog was anesthetized with Fatal-plus (390 mg/ml pentobarbital sodium; 0.2 mg/4.5 kg intravenously). Its heart was quickly removed through a left thoracotomy and immersed in a cold, oxygenated (95% O_2 and 5% CO_2) Tyrode's buffer containing 0.7 mM $MgCl_2$, 0.9 mM NaH_2PO_4, 2.0 mM $CaCl_2$, 124 mM NaCl, 24 mM $NaHCO_3$, 4 mM KCl, and 5.5 mM glucose, pH 7.4. The circumflex coronary artery or a branch of the left anterior descending coronary artery of the heart was cannulated, and a portion of the left ventricle was excised and perfused with the Tyrode's buffer at 37°C for 10–15 min. Afterwards, the perfusion buffer was switched to a Ca^{2+}-free solution containing 118 mM NaCl, 4.8 mM KCl, 1.2 mM $MgSO_4$, 1.2 mM KH_2PO_4, 0.68 mM glutamine, 11 mM glucose, 25 mM $NaHCO_3$, 5 mM pyruvate, 2 mM mannitol, and 10 mM taurine, pH 7.4. Approximately 3–5 min later, collagenase (0.4 mg/ml, type II) and BSA (0.5 mg/ml) were added to the Ca^{2+}-free solution, and perfusion was continued for another 10–12 min. The myocardial tissue was then cut into small pieces and placed in a fresh 10-ml solution of the Ca^{2+}-free buffer with the collagenase and BSA. The digestion mixture was bubbled gently and incubated in a 37°C water bath for 5–10 min. After settlement, the supernatant was discarded, and cardiomyocytes were washed once and incubated at room temperature in a buffer containing 118 mM NaCl, 4.8 mM KCl, 1.2 mM $MgSO_4$, 1.2 mM KH_2PO_4, 0.68 mM glutamine, 11 mM glucose, 25 mM $NaHCO_3$, 5 mM pyruvate, 10 mM taurine, 0.5 mM $CaCl_2$, 2% (w/w) BSA, and 5 mM HEPES, pH 7.4 (buffer A). After 30 min, the isolated cardiomyocytes were washed once more and exchanged into buffer A plus 1 mM $CaCl_2$ (buffer B).

In vitro 2P spectroscopy

Following the analysis by Xu and Webb (1997), the time-averaged 2P fluorescence from an illuminated volume, $\langle F(t)\rangle$, is defined as:

$$\langle F(t)\rangle = \tfrac{1}{2}\,\psi\eta C\delta_{2P}\langle I^2(r,t)\rangle\,, \qquad (1)$$

where η, C, and δ_{2P} are the fluorescence quantum yield, concentration, and 2P-excitation cross section of a fluorophore, respectively; ψ is the instrumental fluorescence collection efficiency; $\langle I(r,t)\rangle$ is the average spatial and temporal profile of the excitation laser pulses. For the same $\langle I(r,t)\rangle$, 2P fluorescence of a reference dye (R) with known δ_{2P} and a fluorophore (U) with unknown δ_{2P} are related by the following equation:

$$\frac{\langle F(t)\rangle_R}{\langle F(t)\rangle_U} = \frac{\psi_R\eta_R C_R\delta_{2P-R}}{\psi_U\eta_U C_U\delta_{2P-U}}\,, \qquad (2)$$

where $\langle F(t)\rangle_R$ and $\langle F(t)\rangle_U$ can be measured by a photomultiplier (PMT); η_R and η_U of 2P excitation are assumed to be the same as those of 1P excitation (Xu and Webb, 1997); ψ is determined by the 1P-fluorescence

emission spectrum of the fluorophore, the transmission properties of the emission filters used, and the quantum efficiency profile of the PMT (Rumi et al., 2000). From Eq. 2, the 2P-excitation action cross section (σ_{2P}) of LipDH, FAD, or NAD(P)H can be determined using the following equation:

$$\sigma_{2P} = \eta_U \delta_{2P-U} = \frac{\psi_R \eta_R C_R \delta_{2P-R} \langle F(t) \rangle_U}{\psi_U C_U \langle F(t) \rangle_R}. \quad (3)$$

In this study, 2P-excitation wavelengths were provided by two Tsunami Ti:sapphire lasers (Spectra Physics, Mountain View, CA) fitted with two mirror sets that cover the respective wavelength ranges of 720–820 nm and 810-1000 nm. The σ_{2P} measurements were carried out using a home-built apparatus. Briefly, the excitation light was focused into a 3 × 3-mm quartz cuvette containing a 100-μl sample using a lens of 17.6-cm focal length. The right-angle 2P fluorescence was imaged onto a Hamamatsu H120–08 PMT (Hamamatsu Corp., Bridgewater, NJ) using a 1:1 telescope system. For 1P- and 2P-emission spectra measurements, an H-10 monochrometer (JY Horiba, Edison, NJ) was inserted between the telescope system and the detector to disperse the fluorescence emission. The monochrometer was calibrated using the 488-, 568-, and 647-nm lines of an Ar-Kr laser. The PMT signal was two-stage amplified using an SR440 amplifier (Stanford Research Systems, Sunnyvale, CA) before being integrated by an SR400 gated photon counter (Stanford Research Systems) for 3 or 5 s. Fluorescein in pH 11 water, whose absolute 2P-excitation cross sections have been published (Xu and Webb, 1996; Albota et al., 1998), was used as the reference dye. A fluorescence quantum yield of 0.9 was used for fluorescein (Demas and Crosby, 1971). The quadratic dependence of 2P fluorescence on the excitation power, 8–10 power levels between 100 and 700 mW, was established at each excitation wavelength, from which the average σ_{2P} and its standard deviation were calculated.

Multiphoton laser scanning microscopy

The multiphoton microscope has been previously described (Williams and Webb, 2000). Briefly, a Zeiss Axiovert-135 inverted microscope (Carl Zeiss, Thornwood, NY) equipped with a Bio-Rad 1024 MP-scanning box (Bio-Rad Laboratories, Hercules, CA) and a Zeiss 40×/1.3 NA F Fluar oil objective was used. For 2P excitation, a Ti:sapphire laser (Millenia-Tsunami combination, Spectra-Physics) provided the 80-MHz mode-locked laser pulses with wavelength selections ranging from 730 to 900 nm. Epifluorescence was separated from the back-scattered excitation light and directed toward the external detectors by a Chroma 670DCLP dichroic mirror (Chroma Technology Corp., Brattleboro, VT). At 750- and 800-nm excitations, the fluorescence emission between 410 and 490 nm was selected by a combination of a Chroma 500DCLP dichroic mirror and a BGG22 band-pass filter, before being detected by a Hamamatsu HC125–02 bialkali PMT (i.e., PMT1; ~410–490 nm). The remaining fluorescence emission between ~510 and 650 nm was selected by a Chroma 670DCLP dichroic mirror and a 575DF150 band-pass filter, before being detected by a second Hamamatsu HC125–02 PMT (i.e., PMT2; ~510–650 nm). For 900-nm excitation, 2P-fluorescence emission below 670 nm was combined by a second 670DCLP dichroic mirror and detected by PMT1 only.

Isolated cardiomyocytes in buffer B were left at room temperature (20–23°C) for at least 1 h before imaging. Subsequently, 200 μl of the cardiomyocyte stock was transferred to a culture dish with a 10-mm diameter coverslip bottom (MatTek Corp., Ashland, MA). After the solution was settled for at least 5 min to allow cell attachment to the glass bottom, an additional 1.8 ml of buffer B was added to bring the final volume to 2 ml. To monitor drug-induced fluorescence changes, five images were acquired at 15-s intervals to establish the baseline autofluorescence intensity. Each image (512 × 768 pixels) was collected by raster scanning the focused laser beam over a typical sample area of ~197 × 296 μm. Each image was acquired in ~1 s, and the average pixel dwell time for the scanning laser beam was ~0.6 μs. Subsequently, 1 ml of buffer B containing 12 mM NaCN, 12 μM FCCP, or 600 μM DNP was added carefully without disturbing the attached cells within the microscopic field of view. Twenty more images were acquired at 15-s intervals immediately after the drug addition. The fluorescence of single cells was integrated using the image analysis program Alice (Perceptive Informatics, Waltham, MA) after subtracting the background intensity (i.e., the average pixel value of images acquired using buffer B only). False color (lookup table: Geog) images were prepared using Confocal Assistant Software (Bio-Rad Laboratories). The weak autofluorescence was enhanced by "contrast stretching" all images to the same extent ($\gamma = 1.8$) and by setting the black level of each image equal to its average background pixel value. Finally, images were edited to appropriate sizes and orientations using Adobe Photoshop 5.5 (Adobe Systems, Inc., San Jose, CA).

Single-cell fluorometry

The multiphoton microscope described above was modified as follows to obtain the 2P-excited autofluorescence emission spectra of single cardiomyocytes. Excitation light at 750, 800, or 900 nm was focused on single cells using an Olympus (Melville, NJ) Uapo/340 40×/1.15 water objective. The epifluorescence was focused by the microscopic tube lens (focal length = 16 cm) and directed by a Chroma 670DCLP dichroic mirror toward a multimode UV-Vis optical fiber with a core diameter of 550 μm (OZ Optics, Carp, Ontario, Canada). A Chroma short-pass filter (HQ680SP) was placed in front of the fiber to further discriminate against the back-scattered excitation light. The fluorescence emission spectra were dispersed using a fiber-coupled 270M-1 spectrometer (Spex, Edison, NJ) equipped with a liquid-N_2-cooled CCD camera. The entrance and exit slit widths of the spectrometer were 3 mm. The wavelength calibration of the system was carried out using the 488-, 568-, and 647-nm lines of an Ar-Kr laser (Bio-Rad Laboratories). Furthermore, the emission spectrum of a model 63358 quartz-tungsten calibration lamp (Oriel Instruments, Stratford, CT) was used to correct for the detection efficiency of the overall system (i.e., the microscope, the optical fiber, the spectrometer, and the CCD) as a function of emission wavelengths. The autofluorescence was integrated for 10 s, and the emission spectrum was corrected based on our calibration of the system. The average excitation power measured after the objective was 8.5, 5.8, or 10.5 mW for 750-, 800-, or 900-nm excitation, respectively. Autofluorescence images were acquired before and after each spectral measurement to ensure normal cellular morphology and absence of abrupt autofluorescence changes during the measurement.

RESULTS AND DISCUSSION

The 2P-ratiometric redox fluorometry based on NAD(P)H and FP fluorescence requires these two signals to be detected at comparable levels when excited using one NIR light. However, the mitochondrial concentration of NADH is orders of magnitude higher than those of fluorescent FPs (i.e., mainly LipDH and ETF) (Guezennec et al., 1991; Kunz and Gellerich, 1993), which typically results in a significant imbalance in their respective fluorescence intensities at one excitation wavelength. Therefore, 2P excitation and detection efficiencies of the FP fluorescence need to be optimized relative to those of the NAD(P)H signal for successful applications of 2P-ratiometric redox fluorometry. Thus, we first determined the 2P characteristics of these intrinsic fluorophores in solution in order to identify the optimal in vivo imaging conditions.

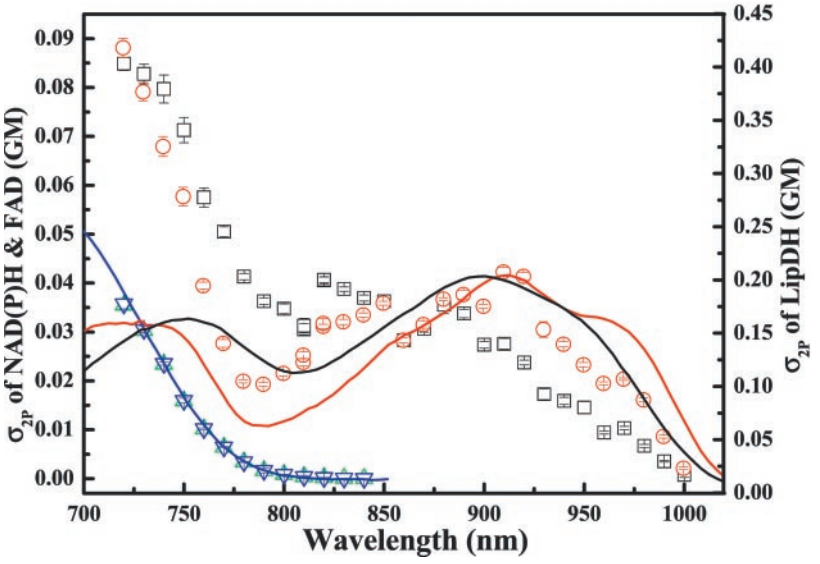

FIGURE 1 Comparison of the 2P-excitation action cross section (σ_{2P}; 1 GM = 10^{-50} cm^4 s) spectra of NADH (*green triangles*) and NADPH (*blue inverted triangles*) to those of FAD (*black squares*) and LipDH (*red circles*; *right axis*). FAD and LipDH have additional 2P-excitation peaks around 900 nm. The 1P-absorption spectra of NADH (*blue line*), FAD (*black line*), and LipDH (*red line*), arbitrarily scaled at twice the excitation wavelengths, are red-shifted related to their 2P counterparts. Error bars are standard deviations of σ_{2P} values determined using 8–10 excitation intensities at each wavelength. Samples are 0.9 μM fluorescein in water (pH 11); 59 μM LipDH in 0.1 M potassium phosphate (pH 7.6) and 0.2 mM EDTA; and 94 μM FAD, 563 μM NADH, and 448 μM NAD(P)H in Tris buffer (pH 7.6).

2P-excitation action cross section measurements

The 2P-excitation action cross section spectra (σ_{2P}) of NAD(P)H, FAD, and LipDH were determined with 10-nm resolution over the wavelength range of 720-1000 nm (Fig. 1). The overall shapes of these 2P spectra are generally predictable from their 1P-absorption spectra (lines, Fig. 1; absorption wavelengths doubled), with the 2P-excitation peaks slightly blue-shifted relative to the 1P peaks. For FAD and LipDH, the 1P-absorption peaks associated with higher energy transitions (i.e., ~376 nm (FAD) and ~363 nm (LipDH)) are slightly smaller than those of lower energy transitions (i.e., ~450 nm (FAD) and ~456 nm (LipDH)). In contrast, the 2P-excitation spectra peak at wavelengths below 720 nm for all molecules examined here. This result is significant because at wavelengths (around 710 nm) previously used for 2P-NAD(P)H excitation (Piston et al., 1995, 1999; Patterson et al., 2000; Kasischke et al., 2001), 2P-FP fluorescence is also maximally excited. Furthermore, the maximum σ_{2P} of LipDH at 720 nm (right *y* axis, Fig. 1) is ~5 and 12 times larger than those of FAD and NAD(P)H (left *y* axis, Fig. 1), respectively. Therefore, although the LipDH concentration in mitochondria is much lower than that of NADH (Guezennec et al., 1991; Kunz and Gellerich, 1993), 2P-ratiometric redox fluorometry may still be possible because of the much larger σ_{2P} of LipDH. On the other hand, at excitation wavelengths longer than 800 nm, there is little 2P-NAD(P)H fluorescence, whereas the 2P-excitation spectra of FAD and LipDH extend up to 1000 nm with broad peaks around 900 nm that are optimal for the selective excitation of FP fluorescence.

In vitro comparison of 1P- and 2P-excited fluorescence emission spectra

The effect of different excitation pathways (i.e., 1P and 2P) on the NAD(P)H, FAD, and LipDH fluorescence are also examined in solution (Fig. 2). The 2P-emission spectra of FAD and LipDH excited at 730 nm (Fig. 2 *A*) and 900 nm (Fig. 2 *B*) are found to be identical to their 1P-excited counterparts (lines, Fig. 2, *A* and *B*). Similarly, the 1P- and 2P-excited emission spectra of NADH have also been shown to be identical by Kierdaszuk et al. (1996); hence, only the 2P-excited spectra of NAD(P)H are shown in Fig. 2 *A*. There is a significant overlap between the emission spectra of NAD(P)H and LipDH, with a crossing point at ~500 nm (Fig. 2 *A*). Therefore, for subsequent imaging experiments, two detectors, PMT1 (~410–490 nm) and PMT2 (~510–650 nm), are set up for maximal NAD(P)H and FP fluorescence detection, respectively. PMT1 detects mostly NAD(P)H signal, whereas PMT2 detects FP fluorescence plus, inescapably, a large NAD(P)H bleed-through.

Cellular 2P-autofluorescence imaging

The ultrastructure of muscle cells is well understood, and both their NAD(P)H and FP fluorescence are predominantly associated with mitochondria (Canale et al., 1986; Eng et al., 1989; Kuznetsov et al., 1998; Saks et al., 1998). Muscle also has the highest content of LipDH among several tissues (i.e., liver, kidney cortex, and brain), and its FP fluorescence has been found to be mostly associated with this protein (Nuutinen et al., 1981; Kunz and Gellerich, 1993; Kunz et al., 1994; Romashko et al., 1998). Consequently, isolated adult dog cardiomyocytes were used in this study to show its 2P-FP fluorescence and were employed as the model system to demonstrate 2P-ratiometric redox fluorometry. The imaging experiments were carried out at room temperature (RT = 20–23°C), which enabled the cardiac cells to maintain good morphology (i.e., rectilinear body with well-defined cell boundaries and few or no cell contractions) for longer than 12 h in buffer B (see Materials and Methods).

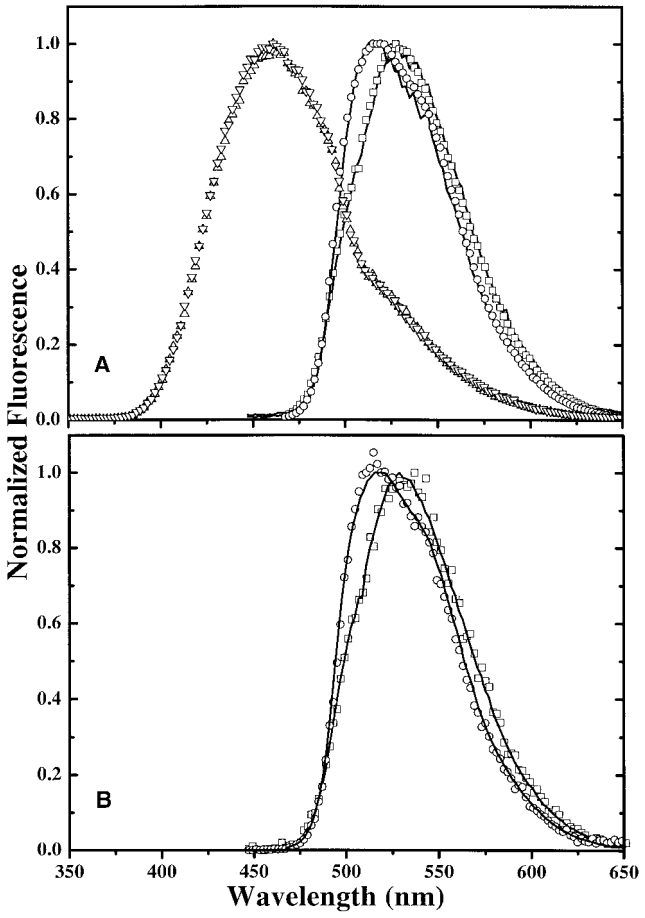

FIGURE 2 The 2P-fluorescence emission spectra of FAD (□) and LipDH (○) at 730-nm (*A*) or 900-nm (*B*) excitation coincide with their 1P counterparts (——). The 2P-emission spectra of NADH (△) and NADPH (▽) are identical and overlap significantly with those of FAD and LipDH (*A*). Spectra shown are not corrected for a small wavelength dependence in the fluorescence detection efficiency of the home-built fluorometer (see Materials and Methods).

The fluorescence quantum yields of NAD(P)H and FPs are slightly enhanced at RT compared with those at the physiological temperature (e.g., NADH fluorescence is enhanced 1.6% with each degree of temperature reduction) (Estabrook, 1962; Chance et al., 1979). Under these conditions, the mitochondria of these cells are also in a relatively oxidized state as prepared, which is beneficial for imaging the weak 2P fluorescence of the oxidized FPs. On the other hand, cellular metabolism at RT is considerably slower than that at the physiological temperature, which likely diminishes the responses of these isolated cardiomyocytes to drugs that alter the mitochondrial metabolic activity (see below).

Because the σ_{2P} spectra suggest that both NAD(P)H and LipDH are 2P excited most efficiently at wavelengths less than 800 nm, cardiomyocytes illuminated with 750-nm light were examined first. High-resolution autofluorescence images were acquired at both PMT1 (Fig. 3 *A*) and PMT2 (Fig. 3 *B*). Comparison of these autofluorescence images to the corresponding transmission image (data not shown) reveals that the autofluorescence distribution aligns well with myofibrillar bundles and is intersected by sarcomeric z-lines. Such compartmentalized fluorescence has been shown for both the 1P-NAD(P)H and FP fluorescence in muscle cells and is found to colocalize with the mitochondria surrounding myofibrils (Eng et al., 1989; Kuznetsov et al., 1998; Romashko et al., 1998). Interestingly, large bright fluorescence spots are also found approximately along the central axis of the cardiomyocyte, where the presence of cellular nuclei disrupts the normal continuation of myofibrils. These hot spots are most likely associated with mitochondrial congregates, as shown below.

To demonstrate the molecular origin of autofluorescence excited at 750 nm, the oxidative phosphorylation inhibitor cyanide (CN) is used to prevent the oxidation of NADH. This results in an increase in the NAD(P)H fluorescence, with a concurrent reduction in the FP signal. Similarly, the mitochondrial uncoupler FCCP produces the opposite changes in the autofluorescence (Eng et al., 1989; Kunz et al., 1994; Kuznetsov et al., 1998; Romashko et al., 1998). The CN and FCCP effects on the autofluorescence images acquired at PMT1 are shown in Fig. 4, with the fluorescence changes indicating a predominantly NAD(P)H signal. These drug-induced changes were examined in further detail by following the evolution of the integrated autofluorescence intensity of single cells after the addition of 4 mM NaCN, 4 μM FCCP, or buffer B only (control). This experiment was repeated for 10–11 different cells to produce the average drug responses of autofluorescence detected at PMT1 (Fig. 5 *A*) and PMT2 (Fig. 5 *B*). An average laser power of ~3.1 mW at the sample was used, resulting in ~5% fluorescence photobleaching during the 350-s time period of monitoring the fluorescence changes (Fig. 5 *A*). This small photobleaching does not produce noticeable damage to the cells as judged by the normal cell morphology (see above) and the absence of abrupt autofluorescence changes (Eng et al., 1989; Bennett et al., 1996; Konig et al., 1996). In Fig. 5 *A*, the addition of CN or FCCP induces a ~34% increase or a ~7% reduction, respectively, indicating that the 2P autofluorescence is predominantly associated with NAD(P)H. Similar drug-induced changes are also observed for the autofluorescence detected at PMT2 (Fig. 5 *B*), albeit with reduced amplitudes (e.g., ~34% CN-induced enhancement at PMT1 versus ~22% at PMT2). These results lead to the conclusion that PMT2 detects mostly the NAD(P)H bleed-through (Fig. 2 *A*) because of the predominantly 2P-NAD(P)H fluorescence excited at 750 nm due to its much higher cellular concentration (Guezennec et al., 1991; Kunz and Gellerich, 1993). On the other hand, the reduced amplitudes of the fluorescence changes observed at PMT2 are likely due to the presence of residual FP signal that responds oppositely to CN or FCCP. Such FP fluorescence is evident upon examining the ratiometric signal $I_r = I_{PMT2}/I_{PMT1}$,

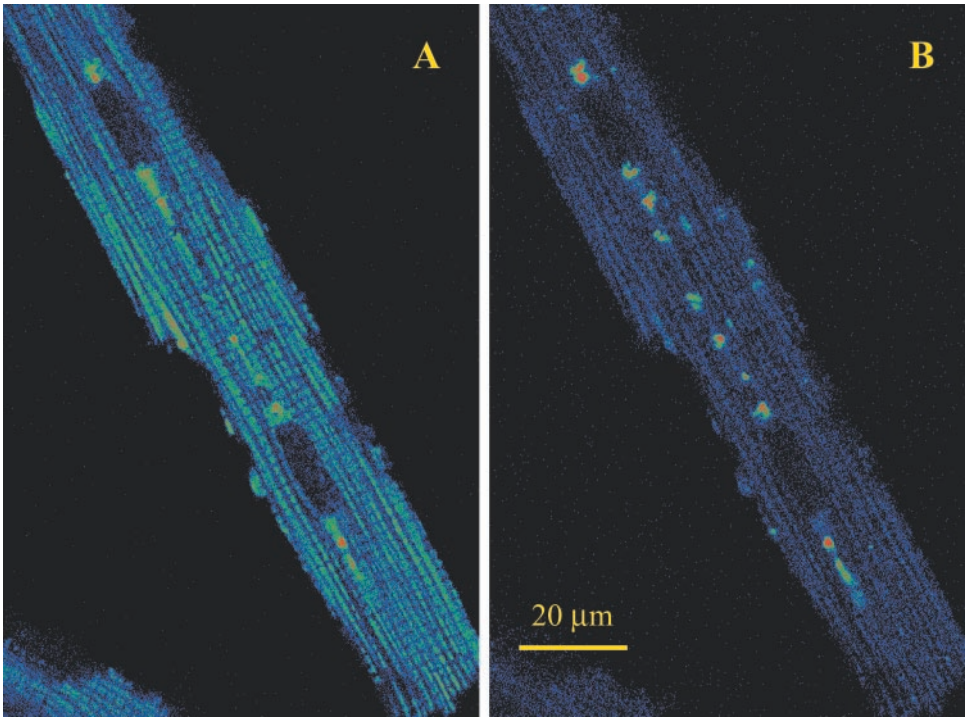

FIGURE 3 At 750 nm excitation, the autofluorescence emission of isolated cardiomyocyte is divided between PMT1 (~410–490 nm) and PMT2 (~510–650 nm), which are set up for maximal detection of the NAD(P)H and FP fluorescence, respectively. The 2P-autofluorescence image obtained at PMT1 (*A*) is much brighter than that at PMT2 (*B*), indicating a predominant NAD(P)H signal. Images shown are the average of five consecutive scans.

where I_{PMT2} and I_{PMT1} are the fluorescence intensities registered at PMT2 and PMT1, respectively. At 750-nm excitation, I_{PMT1} contains mostly the NAD(P)H fluorescence (I_N) and a small FP cross-over (I_{FC}), whereas I_{PMT2} includes

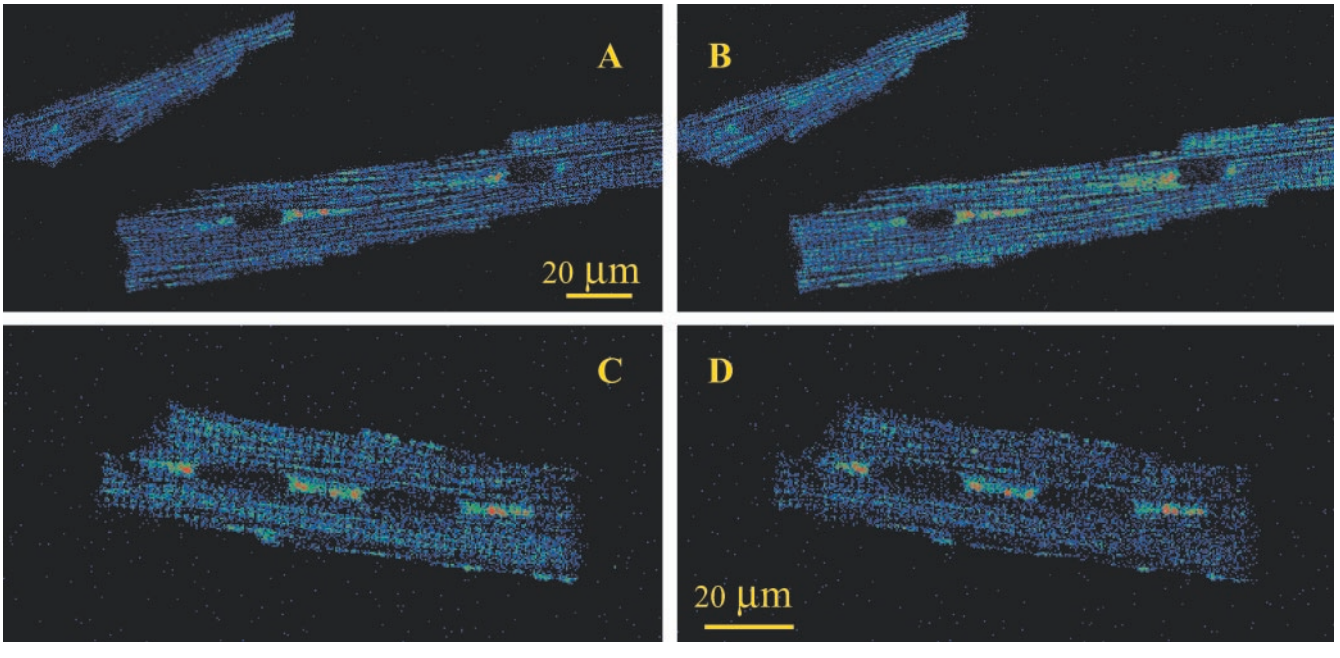

FIGURE 4 Addition of 4 mM NaCN (*A* and *B*) or 4 μM FCCP (*C* and *D*) to the cardiomyocytes induces autofluorescence enhancement or reduction, respectively. Images *A* and *C* were acquired immediately before the addition of drugs, whereas *B* and *D* were acquired 55 and 10 s after the addition of NaCN or FCCP, respectively. Autofluorescence was excited at 750 nm and collected by PMT1 (~410–490 nm) without averaging.

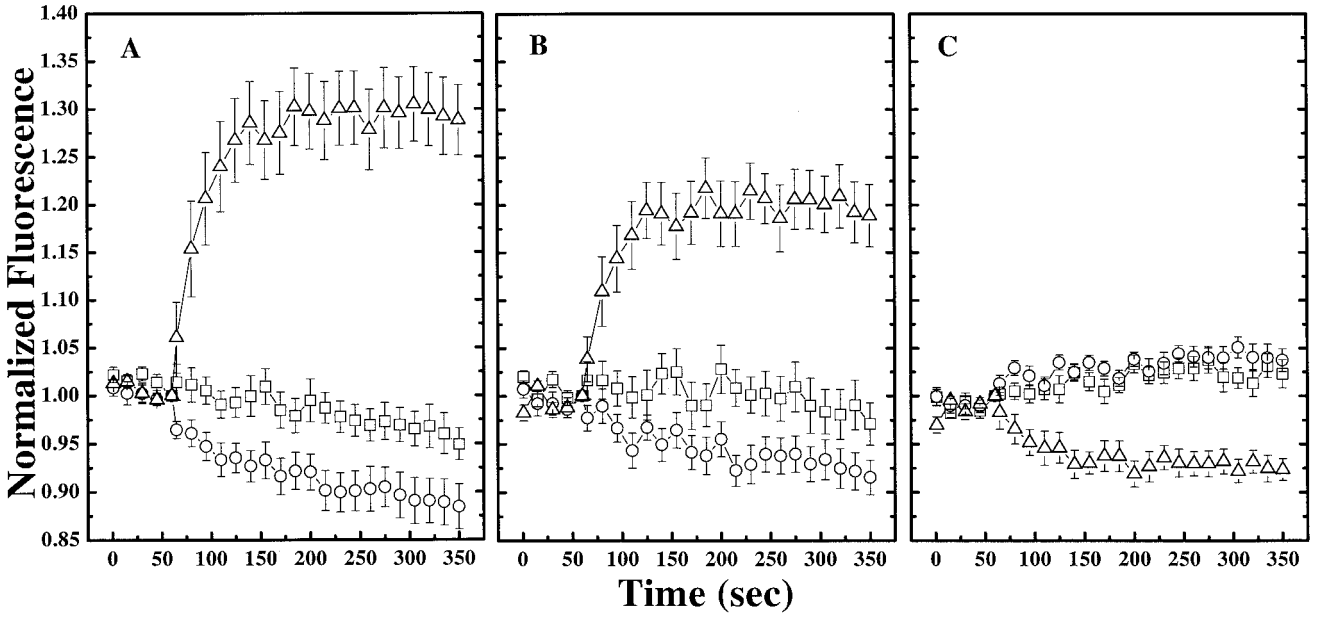

FIGURE 5 The time dependence of autofluorescence (λ_{ex} = 750 nm) changes induced by 4 mM CN (△), 4 μM FCCP (○), or buffer B only (control; □). (*A*) Autofluorescence detected at PMT1 (~410–490 nm; I_{PMT1}); (*B*) Autofluorescence detected at PMT2 (~510–650 nm; I_{PMT2}); (c) Ratiometric signal $I_r = I_{PMT2}/I_{PMT1}$. The integrated fluorescence intensity of individual cells is normalized to that immediately before the addition of drugs (at 60 s). Error bars represent the standard errors of the mean for measurements of 10–11 different cells.

both the FP signal (I_F) and a large NAD(P)H bleed-through (I_{NC}; Fig. 2 *A*), yielding a ratio $I_r \approx (I_F + I_{NC})/I_N = I_F/I_N + I_{NC}/I_N$. Because I_{NC}/I_N is constant, addition of CN decreases I_r by enhancing I_N and quenching I_F, as observed in Fig. 5 *C*. However, the large amplitude of the CN effect on the 2P-NAD(P)H fluorescence (Fig. 5 *A*) is reduced by ~3-fold for I_r (Fig. 5*C*), because $I_F/I_N \ll I_{NC}/I_N$. For the smaller FCCP effect, its corresponding change in I_r is negligible (Fig. 5 *C*). Therefore, despite a much larger σ_{2P} for LipDH, the autofluorescence excited at 750 nm is dominated by NAD(P)H emission, in agreement with previous studies where 2P-NAD(P)H fluorescence is predominantly detected at 710-nm excitation (Piston et al., 1995, 1999; Patterson et al., 2000).

To realize 2P-ratiometric redox fluorometry, difficulties related to the concentration disparity between the NAD(P)H and FP molecules must be overcome. The 2P-excitation spectra (Fig. 1) indicate that the σ_{2P} of NAD(P)H decreases to a negligible level whereas that of LipDH is reduced by ~60% when the excitation wavelength is increased from 750 nm to 800 nm. In fact, 2P excitation of LipDH is ~130 times more efficient than that of NAD(P)H at 800 nm, according to their respective σ_{2P} values. Therefore, it is feasible to compensate for the difference in the NAD(P)H and LipDH concentrations, hence their respective fluorescence intensities, by imaging the cardiomyocytes under 800-nm illumination (Fig. 6). A higher excitation power of ~8.8 mW at the sample was used compared with the ~3.1 mW used at 750 nm. Nevertheless, a substantially dimmer autofluorescence image is obtained at PMT1 (Fig. 6 *A*) compared with its counterpart at 750-nm excitation (Fig. 3 *A*), which reflects a corresponding large decrease in the σ_{2P} of NAD(P)H (Fig. 1). On the other hand, the autofluorescence image obtained at PMT2 is slightly brighter (Fig. 6 *B* compared with Fig. 3 *B*), suggesting a small enhancement in the FP signal. This enhancement is caused by the quadratic dependence of 2P-FP fluorescence on the higher excitation power used at 800 nm, which overcomes a corresponding ~60% decrease in the σ_{2P} of LipDH (Fig. 1). Overall, the integrated fluorescence intensity ratio I_{PMT1}/I_{PMT2} decreases from 4.1 (Fig. 3) to 1.8 (Fig. 6), reflecting a reduction in the NAD(P)H fluorescence but an enhancement in the FP signal at 800-nm excitation. Thus, relatively balanced FP and NAD(P)H signals can be achieved by the optimal selection of the excitation wavelength for 2P-ratiometric redox measurement.

The above conclusion is further supported by the average drug responses of seven to eight cells shown in Fig. 7. The higher excitation power results in a ~12% fluorescence bleaching in 350 s for the control sample (Fig. 7 *A*). Nevertheless, the cells maintain their normal morphology without abrupt autofluorescence changes associated with cell deterioration. At PMT1 (Fig. 7 *A*), the addition of CN eventually induces a ~21% fluorescence enhancement whereas FCCP induces a ~17% reduction, indicating a predominant 2P-NAD(P)H signal. In contrast, much smaller drug effects are observed at PMT2 (Fig. 7 *B*), which is likely due to the relatively comparable levels of FP and

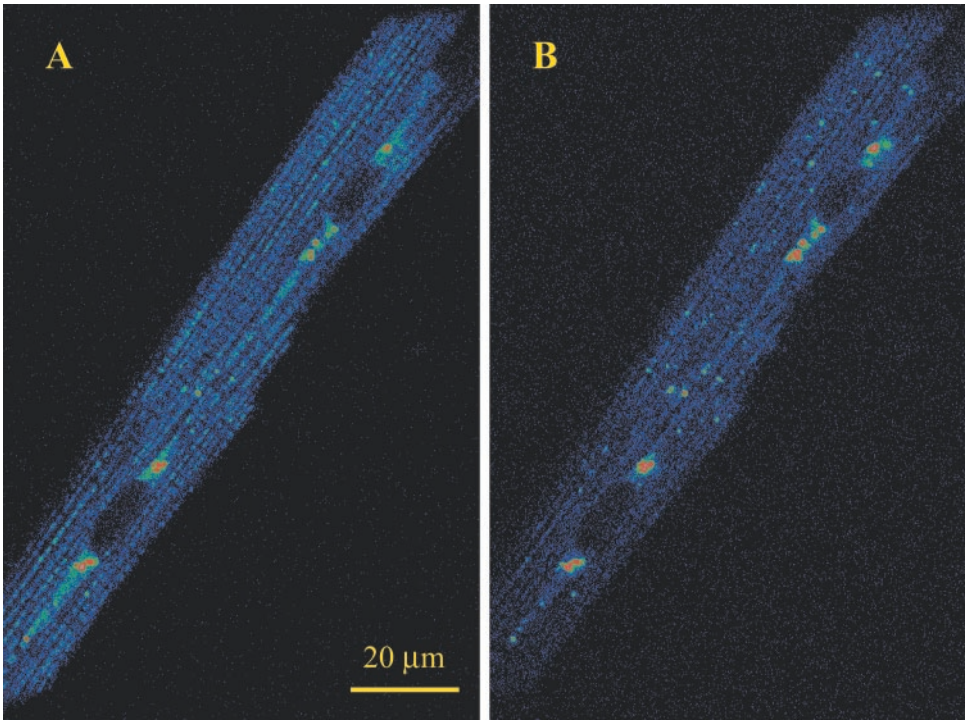

FIGURE 6 At 800-nm excitation, 2P-autofluorescence images of relatively comparable brightness were obtained at PMT1 (~410–490 nm; *A*) and PMT2 (~510–650 nm; *B*), indicating the presence of both the NAD(P)H and FP signals. Images were the average of five consecutive times.

NAD(P)H fluorescence detected at this channel. These two signals respond oppositely to CN or FCCP, thus canceling out each other's drug responses. The drug-induced changes are largely recovered upon examining the ratiometric signal I_r (Fig. 7 *C*). Directions of changes in I_r are opposite to those observed for the 2P-NAD(P)H fluorescence (Fig. 7 *A*) but are consistent with the above analysis of this ratiometric signal. Therefore, Fig. 7 *C* demonstrates the feasibility of

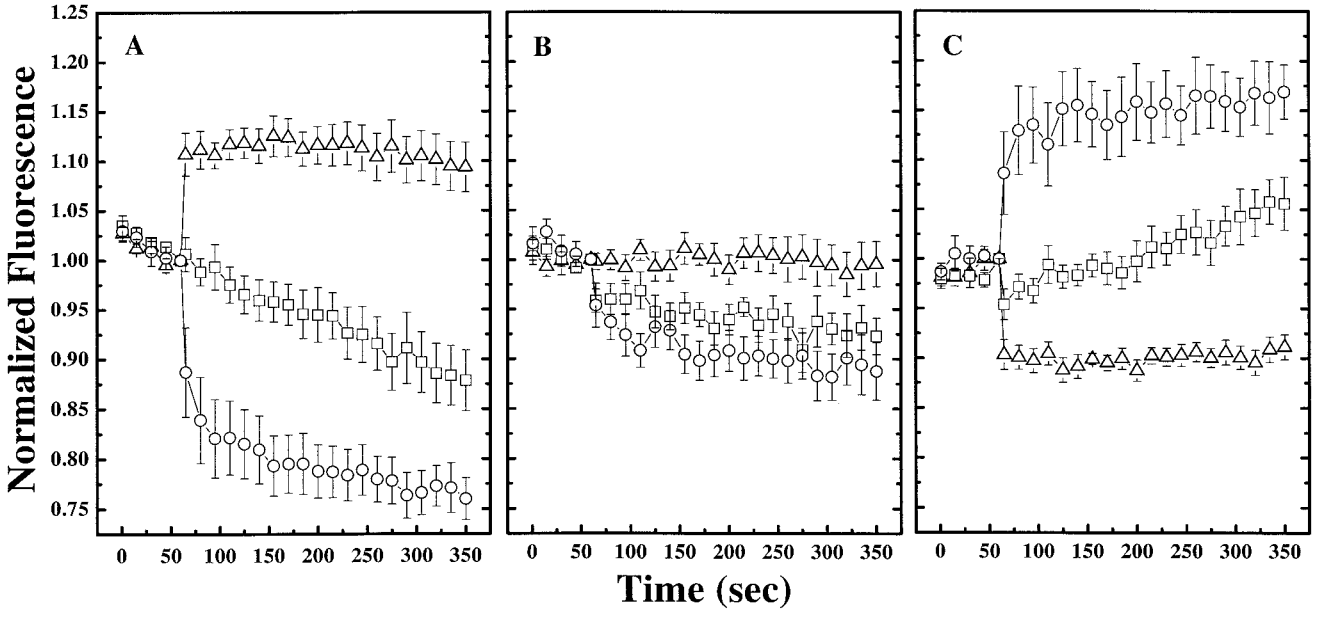

FIGURE 7 The time dependence of 2P-autofluorescence (λ_{ex} = 800 nm) changes induced by 4 mM CN (△), 4 μM FCCP (○), or buffer B only (control; □). (*A*) Autofluorescence detected at PMT1 (~410–490 nm; I_{PMT1}); (*B*) Autofluorescence detected at PMT2 (~510–650 nm; I_{PMT2}); (*C*) Ratiometric signal $I_r = I_{PMT2}/I_{PMT1}$. Error bars are the standard errors of the mean of seven to eight measurements using different cells.

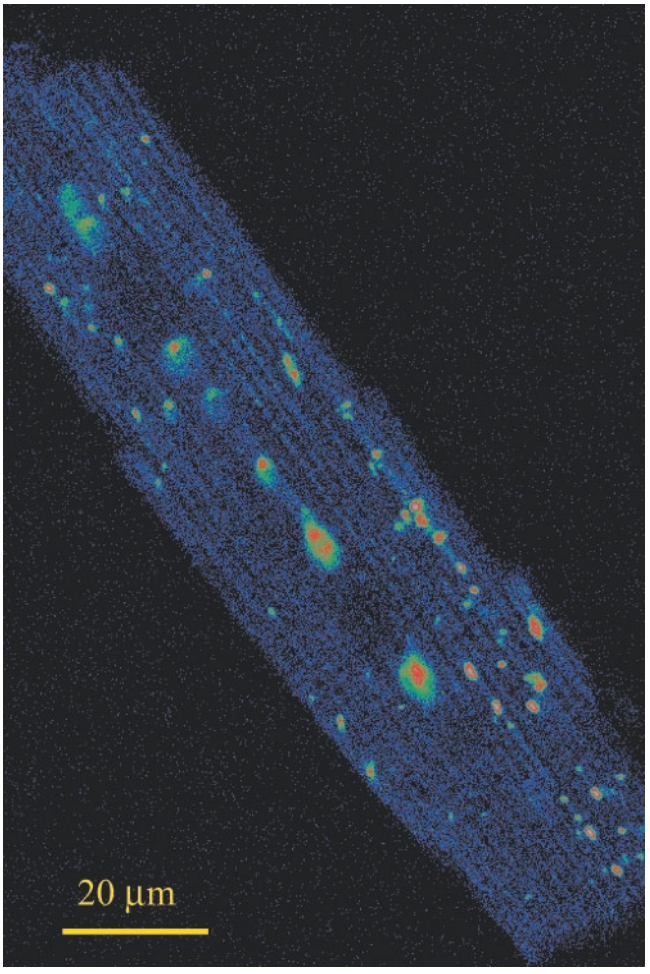

FIGURE 8 A 2P-autofluorescence image of adult dog cardiomyocyte excited at 900 nm. The weak autofluorescence emission was combined and detected by PMT1 (< 650 nm; see Materials and Methods) only. The image was produced by averaging five consecutive scans.

2P-ratiometric redox fluorometry at 800-nm excitation, which can be further improved as discussed below.

Finally, the σ_{2P} data in Fig. 1 indicate that only FAD and LipDH are efficiently 2P excited at 900 nm. Therefore, the weak autofluorescence emission of the cardiomyocyte excited at 900 nm was combined and detected by PMT1 only (Fig. 8). In general, the resulting autofluorescence image is similar to those obtained at 750 and 800 nm (Fig. 3 and 6), except that there are more hot spots observed under 900-nm illumination. These hot spots with significantly elevated pixel intensities can be classified into two categories. Small ones of 1–2 μm distribute randomly throughout the cell and are comparable in size to individual cardiac mitochondria (Dow et al., 1981; Segretain et al., 1981). Such small hot spots have been observed in isolated guinea pig cardiomyocytes using the 1P-excited FP fluorescence and are attributed to the highly oxidized individual mitochondria (Romashko et al., 1998). There are also larger 2–5-μm hot spots, which are primarily found at the polar regions surrounding the cardiomyocyte nuclei (i.e., cigar-shaped dark regions along the central axis of cardiomyocyte; Figs. 3, 6, and 8). Electron microscopic images of cardiomyocytes reveal various cellular organelles at these perinuclear polar regions, including significant amounts of mitochondria, as well as Golgi apparatuses, lipofuscin granules, and lysosomes (Canale et al., 1986). To understand which cellular organelle contributes most to the intense autofluorescence observed at these polar regions, the average CN effect associated with three large hot spots (within squares, Fig. 9 *A*) is compared with that of three representative normal regions (within circles, Fig. 9 *A*). Both the time-dependent fluorescence enhancements of the normal regions and the hot spots coincide well with that of the integrated fluorescence intensity of the whole cell, except for a small time delay (i.e., ~50 s) for the onset of the CN effect for the hot spots (Fig. 9 *B*). This delay probably reflects CN diffusion within the cardiomyocyte. Similar analysis is performed for cardiomyocytes excited at 800 nm and 900 nm, and essentially the same result shown in Fig. 9 is obtained. Therefore, the intense autofluorescence of these large hot spots most likely originates from mitochondrial congregates at the polar regions adjacent to the cardiac nucleus (Canale et al., 1986). Nevertheless, fluorescence contributions from age-related lipofuscin granules and degraded protein debris within lysosomes, which are insensitive to CN or FCCP, cannot be completely ruled out. However, any such contributions are negligible compared with the integrated fluorescence intensity of the whole cell, as demonstrated by the concurrence of the CN effects derived from analysis using either the integrated whole-cell intensity or the intensity excluding the large hot spots (Fig. 10).

The molecular origin of the 2P autofluorescence excited at 900 nm was further examined by the addition of CN or FCCP, which resulted in a ~12% fluorescence reduction or a ~2–3% fluorescence enhancement, respectively (Fig. 10). The directions of these autofluorescence changes are opposite to those observed for the 2P-NAD(P)H fluorescence (Figs. 5 *A* and 7 *A*) but consistent with the 2P-FP signal. Amplitudes of these drug effects (Fig. 10) are two to three times smaller than those observed for the NAD(P)H signal (Figs. 3 *A* and 6 *A*). Such minor drug effects associated with the FP fluorescence have also been observed in isolated rat liver mitochondria (Chance et al., 1979) and are likely due to the following facts. First, the dithiothreitol-reducible FP signal (see Introduction) is insensitive to drugs that alter the mitochondrial metabolic states (Kunz and Kunz, 1985; Kunz, 1986). Second, two-electron reduced LipDH (i.e., $FADH_2$) preserves ~15% of the flavin fluorescence of the oxidized enzyme (i.e., FAD) (Veeger et al., 1976). Third, NAD^+ binding to the oxidized LipDH decreases its flavin

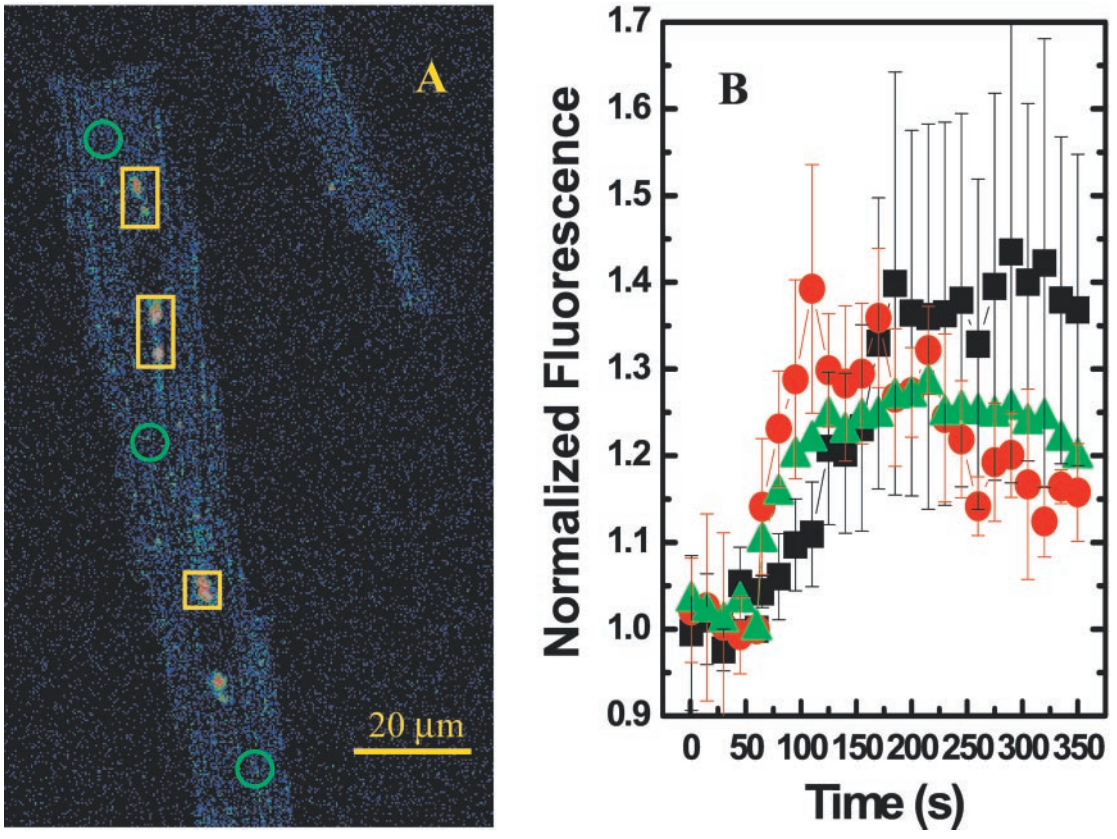

FIGURE 9 Analysis of the large hot spots in the polar perinuclear regions of adult dog cardiomyocyte. (*A*) Autofluorescence excited at 750 nm was collected at PMT2 (~510–650 nm) without averaging, resulting in a noisy background with an average pixel intensity of 12. Representative large hot spots were selected by squares and normal regions by circles. (*B*) The CN-induced autofluorescence changes associated with the hot spots (■) and normal regions (●) are compared with that of the integrated fluorescence intensity of the whole cell (▲). Error bars are the standard errors of the mean.

fluorescence (Maeda-Yorita and Aki, 1984). Fourth, the redox state of ETF is indirectly affected by the mitochondrial NAD^+/NADH ratio (see Introduction) (Kunz, 1988). Finally, at 900-nm excitation, background autofluorescence

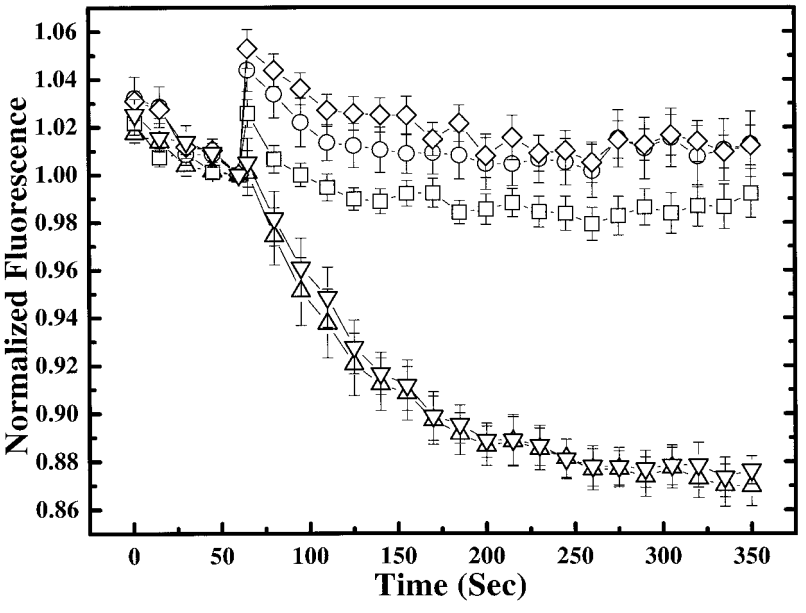

FIGURE 10 The time dependence of 2P-autofluorescence (λ_{ex} = 900 nm) changes induced by addition of 4 mM NaCN (△), 4 μM FCCP (○), 200 μM DNP (◇), or incubation buffer only (control; □). The CN effect was also analyzed using the integrated fluorescence intensity of single cells excluding the large hot spots (▽). Error bars are the standard errors of the mean of 12–15 independent measurements. The autofluorescence emission was combined and detected by PMT1 (<650 nm) only. There is an elevated dark current in PMT1 immediately after the addition of drugs, producing an initial apparent enhancement in the autofluorescence signal. This artifact is due to exposure of the detector to room light that is necessary during drug addition. Such transient enhancement is less obvious in Figs. 5 and 7 because of different plotting scales and because the detectors are better protected by additional band-pass filters used in those experiments (see Materials and Methods). The average amplitude of this artificial enhancement is constant throughout the experiment and decays away in less than 30 s.

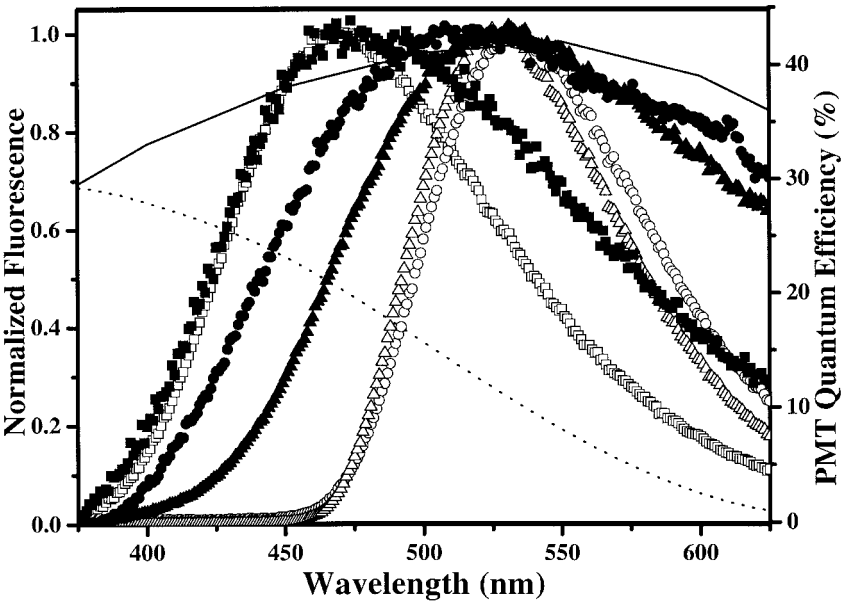

FIGURE 11 The 2P-excited autofluorescence emission spectra of single cardiac cells were obtained at 750-nm (■), 800-nm (●), and 900-nm (▲) excitation. For comparison, the in vitro 2P-emission spectra of NADH (□) excited at 750 nm and LipDH (○) excited at 900 nm were also obtained under the same experimental conditions. Fluorescence emission from the incubation buffer alone is negligible and thus is not included in this figure. Spectra shown are corrected for the wavelength-shift and wavelength-dependent variations in the detection efficiency of the microscope-based fluorometer (see Materials and Methods). The quantum efficiency profiles (supplied by Hamamatsu Corp., Bridgewater, NJ) of bialkali PMT (i.e., PMT1 and 2; · · ·) and GaAsP PMT (——) are also included.

other than the 2P-FP signal may also contribute to the smaller drug effects (see below). Despite these complications, a small FCCP-induced fluorescence enhancement is resolved, which is repeated with another mitochondrial uncoupler, 2,4-dinitrophenol (Fig. 10). An average laser power of ~12.8 mW at the sample was used to excite the weak FP fluorescence. However, the cells maintained their normal morphology throughout the experiment. There is also negligible fluorescence photobleaching (Fig. 10), consistent with previous observation that FPs are significantly more resistant to photobleaching than NAD(P)H (Scholz et al., 1969). Finally, it is concluded that 900-nm excitation is most suitable for detecting 2P-FP fluorescence.

2P-autofluorescence emission spectra of single cardiomyocytes

The molecular origins of autofluorescence excited at 750, 800, and 900 nm are also confirmed by the 2P-autofluorescence emission spectra of single cardiomyocytes (Fig. 11). For comparison, the 2P-emission spectra of NADH and LipDH in solution are also obtained under the same experimental conditions (Fig. 11). At 750-nm excitation, the cellular spectrum coincides well with the in vitro spectrum of NADH, except for a substantial enhancement in the red emission at wavelengths >490 nm that can be attributed to the FP fluorescence. This result agrees with the σ_{2P} measurements that suggest both the NAD(P)H and FP molecules are efficiently 2P excited at 750 nm (Fig. 1). Comparison of the in vivo and in vitro spectra further demonstrates that the cellular NAD(P)H emission dominates at this excitation wavelength (Fig. 11), which is consistent with the drug effects shown in Fig. 5. Indeed, assuming that the difference between the in vitro and in vivo spectra is solely due to the FP signal, it can be estimated that ~62% of the cellular autofluorescence emission between 510 and 625 nm (i.e., within the detection spectral window of PMT2) is composed of the NAD(P)H bleed-through. Because the CN effects on the relatively pure NAD(P)H (Fig. 5 *A*) and FP (Fig. 10) signals are ~34% and ~12%, respectively, the expected CN effect on the autofluorescence detected at PMT2 ($I_{PMT2} = I_F + I_{NC}$; see above) can be calculated to be ~17%. Considering significant variations in the drug responses of individual cells, this calculated CN effect is in close agreement with the average result of ~22% derived from experimental measurements of 10–11 cells (Fig. 5 *B*).

The cellular spectrum obtained at 900-nm excitation is significantly red-shifted and peaks at about the same wavelength as the in vitro spectrum of LipDH (Fig. 11). However, the cellular spectrum is significantly broader, reflecting the complexity in the composition of cellular FP fluorescence that includes contributions from not only LipDH and ETF but also flavins that are reducible only in the presence of DIT (see Introduction). Such broad cellular FP fluorescence spectrum has also been observed using 1P excitation (Chance and Lieberman, 1978; Chance et al., 1979; Kunz, 1986; Kunz et al., 1994). Interestingly, a small amount of autofluorescence emission at wavelengths <450 nm is observed, which cannot be caused by 2P excitation at 900 nm, because the energy of the fluorescence photon would be larger than the sum of the energy of two excitation photons. Several factors may contribute to this unexpected blue emission. First, the excitation pulse width (i.e., full width half-maximum ≈ 15 nm) at 900 nm introduces some of the blue emission below 450 nm. Second, 3P-excited autofluorescence can emit below 450 nm. A considerable amount of

3P autofluorescence has been reported for in vivo human skin excited at 960 nm (Masters et al., 1997). However, 3P autofluorescence is not expected under our imaging conditions, unless there are unidentified intrinsic fluorophores with exceptionally large 3P-excitation cross sections within the isolated cardiomyocytes. This unexpected blue autofluorescence is unlikely due to 3P excitation of FAD and LipDH, because both molecules have negligible fluorescence quantum yields at 300 nm (i.e., 1P equivalent of 3P excitation at 900 nm). Thus, the molecular origin of this potential 3P fluorescence awaits further investigation. Finally, the fluorescence detection efficiency of the liquid-N_2-cooled CCD camera used for spectral acquisition (see Materials and Methods) peaks at ~562 nm. Therefore, autofluorescence emission on both sides of this peak wavelength needs to be compensated based on our calibration of the microscope-based spectrophotometer. Consequently, a small variation in the calibration curve at wavelengths <450 nm may artificially boost the autofluorescence emission. In fact, for the uncorrected emission spectrum, there is a negligible amount of fluorescence emission below 450 nm. Despite the above complications, comparison of the cellular emission spectrum with that of LipDH demonstrates that the cellular FP fluorescence dominates at 900-nm excitation.

Finally, at 800-nm excitation, the cellular spectrum resembles that measured at 900 nm, except for a significant enhancement at wavelengths <510 nm that can be attributed to the NAD(P)H emission. This result is consistent with the σ_{2P} measurements that indicate negligible 2P excitation for NAD(P)H but substantial 2P excitation for LipDH at 800 nm (Fig. 1). The cellular FP fluorescence appears to dominate at this excitation wavelength, but the NAD(P)H contribution may be underestimated because of its much faster photobleaching rate during the 10-s integration time that is necessary to acquire the emission spectrum (see Materials and Methods). Furthermore, a quantitative estimation of the NAD(P)H contribution is not possible here, because of the uncertainty associated with the cellular FP fluorescence spectrum obtained at 900 nm. The conditions that introduce the unexpected blue emission (see above) may not be present at 800-nm excitation. In fact, only a tiny amount of autofluorescence emission at wavelengths <400 nm is observed for 800-nm excitation. With these considerations and because the NAD(P)H fluorescence is much more sensitive to changes in the mitochondrial metabolic states (see above), the NAD(P)H-like drug effects are observed at PMT1 (~410–490 nm) with the amplitudes of fluorescence change reduced by a likely substantial FP cross-over (Fig. 7 *A*). At PMT2 (~510–670 nm), the drug effects of NAD(P)H and FP fluorescence mostly cancel each other out (Fig. 7 *B*).

Finally, the emission spectra shown in Fig. 11 suggest that the detection specificity for both the NAD(P)H and FP fluorescence can be improved by narrowing the spectral windows of PMT1 (i.e., 410–490 nm) and PMT2 (i.e., 510–640 nm). For example, the spectral window for detecting the FP fluorescence may start from 550 nm to avoid most of the NAD(P)H bleed-through. Such an approach will be feasible using a detector with higher detection quantum efficiencies (i.e., GaAsP PMT) than the one used in this study (i.e., bialkali PMT; see below). For comparison, the quantum efficiency (QE) profiles of both PMTs are included in Fig. 11 (right axis).

Summary and future developments

Redox fluorometry based on the intrinsic NAD(P)H and/or FP fluorescence provides a minimally invasive way of monitoring cellular energy metabolism as a function of substrate availability, oxygen supply, or mitochondrial function deficiencies (reviewed by Balaban and Mandel, 1990; Chance, 1991; Masters and Chance, 1993; Saks et al., 1998). However, when applied to in situ monitoring of tissue or organ metabolism, redox fluorometry suffers from problems associated with light scattering in turbid biological environment, light absorption by intrinsic pigments (i.e., hemoglobin, myoglobin, cytochromes, etc.), nonspecific background fluorescence, blood flow, sample movement, and instrumental instability. Consequently, ratiometric redox fluorometry based on both the NAD(P)H and FP fluorescence has been proposed to provide an internal calibration against the above interfering factors (Chance et al., 1978; Quistorff et al., 1985). However, at UV and visible wavelengths for 1P excitation, light intensity and signal integrity quickly degrade as a function of sample depth, so that only the surface autofluorescence can be collected and analyzed reliably. To achieve three-dimensional resolution, tissues have been frozen at liquid nitrogen temperature and mechanically sliced to expose the subsequent cell layers. This method typically provides >100-μm resolution so that metabolic information of individual cells is not attainable (Masters, 1984; Quistorff et al., 1985). Attempts to integrate redox fluorometry with high-resolution fluorescence microscopy have been made (reviewed by Masters, 1984; Masters and Chance, 1993), particularly with confocal and multiphoton microscopy (MPM), which provide submicron lateral resolution and three-dimensional section capability (Kuznetsov et al., 1998; Romashko et al., 1998; Patterson et al., 2000; Kasischke et al., 2001). However, the complexity of the 1P-ratiometric redox fluorometry (e.g., two excitation lights, time-sharing excitation, and detection devices) prevents its easy integration with the confocal microscopic configuration. On the other hand, with MPM, both the NAD(P)H and FP fluorescence can be simultaneously 2P excited at one NIR wavelength (Figs. 1, 7 and 11), so that complications related to the different inner-filter and light-scattering ef-

fects of two-color 1P excitation are avoided. Furthermore, MPM provides much improved optical section capability in highly scattering biological media compared with confocal microscopy, as exemplified by its ability to resolve subcellular structures at depth >200 μm in brain slice and >400 μm in rabbit cornea (Piston et al., 1995; Kasischke et al., 2001). Finally, previous ratiometric redox techniques cannot differentiate the mitochondrial NADH fluorescence from the cytosolic NAD(P)H signal, which complicates the analysis of the FP/NAD(P)H ratio signal and reduces the sensitivity of the technique toward changes in mitochondrial metabolic activity (Masters, 1984; Quistorff et al., 1985). However, with submicron resolution provided by MPM, individual mitochondria are resolved (Fig. 8) so that mitochondrial NADH fluorescence can be isolated (Patterson et al., 2000). Therefore, 2P-ratiometric redox fluorometry may be applied to individual mitochondria with enhanced sensitivity. In conclusion, the above and other advantages of MPM (see Introduction; reviewed by Denk et al., 1995; Xu et al., 1996) make it an attractive approach for ratiometric redox fluorometry. However, a major difficulty of any ratiometric redox technique is caused by the concentration disparity of the mitochondrial NADH and FP molecules. Furthermore, with 2P excitation at one NIR wavelength, it is difficult to completely separate the overlapping NAD(P)H and FP signals (Figs. 2 and 11). Additional challenges are the small excitation cross sections of the intrinsic fluorophores (Fig. 1) and the low quantum efficiency of PMT in detecting the FP fluorescence (Fig. 11). These difficulties provide motivations to further improve the 2P-ratiometric redox technique.

Effective application of autofluorescence to biological studies relies on good understanding of the photophysics of the intrinsic fluorophores involved. In this study, the 2P characteristics of NAD(P)H, FAD, and LipDH are systematically examined in solution over a wavelength range that is important for MPM (Figs. 1 and 2). These in vitro results provide not only the strategy of imaging 2P-NAD(P)H, FP, or both types of fluorescence in isolated adult dog cardiomyocytes, but also a guideline for minimizing the autofluorescence background during multiphoton excitation of extrinsic fluorophores. The σ_{2P} values of NAD(P)H and FAD determined in this study are extensions to those previously measured by Xu et al. (1996), which cover the wavelength range of 690–800 nm only. Those early data are repeated, for the purpose of quantitative comparison, under the same experimental conditions under which the new measurements for LipDH and FAD were carried out. More importantly, additional 2P-excitation peaks around 900 nm are discovered for FAD and LipDH, which leads to the first confirmed image of 2P cellular FP fluorescence (Fig. 8). The σ_{2P} values shown in this study are comparable to those determined by Xu et al. (Xu et al., 1996; Xu and Webb, 1997).

For non-centrosymmetric fluorophores such as NAD(P)H and FAD, a transition to the lowest excitation state (S_1 state) can be achieved through either the 1P or 2P processes (Xu and Webb, 1997; Wakebe and van Keuren, 1999). Therefore, the 2P-excitation spectra of these molecules can be largely predictable from their 1P counterparts (Fig. 1). Furthermore, the 2P- and 1P-fluorescence emission spectra are exactly the same (Fig. 2), which is expected because both result from the same S_1 state (i.e., Kasha's Rule; Kierdaszuk et al., 1996; Xu and Webb, 1997). Consequently, the 2P excitation and emission properties of another important FP, ETF (see Introduction), which is not characterized in this study because of its lack of ready availability, can be speculated. The 1P absorption and fluorescence emission peaks of ETF are blue-shifted by ~20 and 30 nm compared with those of LipDH, respectively (Hall and Kamin, 1975). Therefore, ETF should also be 2P excited at wavelengths used in this study, and its fluorescence probably contributes to the broadening on the blue side of the cellular autofluorescence emission spectrum determined at 900 nm (Fig. 11). By the same argument, the dithiothreitol-reducible FPs (see Introduction) likely also contribute to the broadening of the 2P-cellular emission spectrum obtained at 900-nm excitation (Fig. 11; Kunz and Kunz, 1985; Kunz, 1986). Consequently, not only the FP fluorescence detected at PMT2 is contaminated by a large NAD(P)H bleed-through but also the NAD(P)H signal at PMT1 by a substantial FP crossover, especially at 800 nm proposed for 2P-ratiometric redox fluorometry (Fig. 1 and 11). Thus, a more effective way of separating the NAD(P)H and FP fluorescence is needed.

The average fluorescence lifetime of LipDH in solution is determined to be 4.55 ns, which is approximately nine times larger than that of NADH (0.51 ns; data not shown), suggesting that these two signals may be effectively separated in the lifetime domain. Therefore, a time-gated fluorescence detector that can selectively accumulate the NAD(P)H and FP photons at different time windows following each 2P-excitatoin pulses (pulse width $\approx$ 100 fs) will significantly improve the sensitivity of the 2P-ratiometric redox method. Furthermore, as demonstrated in Fig. 11, the detection efficiency for both the NAD(P)H and the FP fluorescence can be substantially improved. At 470 and 525 nm, emission peaks for the NAD(P)H and FP (i.e., ~525 nm) fluorescence, respectively, the quantum efficiencies (QEs) of the GaAsP PMT are ~1.4 and ~3.7 times higher than the corresponding QEs of the bialkali PMT used in this study. Although this recently available GaAsP PMT can operate only in the photon-counting mode that is not suitable for high-intensity fluorescence imaging, it may be sufficient for the weak intrinsic fluorescence of NAD(P)H and FP. Such a PMT will enhance the FP fluorescence relative to the NAD(P)H signal, thus significantly improving the sensitivity of 2P-ratiometric redox measurement. Finally, we conclude that future technical advancements (e.g., lifetime-

based autofluorescence detection and GaAsP PMT) will substantially improve the 2P-ratiometric technique, whose potential is explored here only as a proof of principle.

We thank Dr. Robert Gilmour and Fei Hua at Cornell Veterinary College for preparing the isolated adult dog cardiomyocytes. We also thank Harsh Vishwasrao for helping us to obtain the single-cell autofluorescence emission spectra and Dr. Karl Kasischke for thoughtful discussions.

This project was carried out in the Biomedical Technology Resource, Developmental Resource for Biophysical Imaging Opto-electronics, and the publication was made possible by grant P41-RR04224 from the National Center for Research Resources, National Institutes of Health (Bethesda, MD).

REFERENCES

Albota, M. A., C. Xu, and W. W. Webb. 1998. Two-photon fluorescence excitation cross sections of biomolecular probes from 690 to 960 nm. *Appl. Opt.* 37:7352–7356.

Balaban, R. S., and L. J. Mandel. 1990. Optical methods for the study of metabolism in intact cells. *In* Noninvasive Techniques in Cell Biology. J. K. Foskett and S. Grinstein, editors. Wiley-Liss, New York. 213–236.

Bennett, B. D., T. L. Jetton, G. Ying, M. A. Magnuson, and D. W. Piston. 1996. Quantitative subcellular imaging of glucose metabolism within intact pancreatic islets. *J. Biol. Chem.* 271:3647–3651.

Berger, I., O. N. Elpeleg, and A. Saada. 1996. Lipoamide dehydrogenase activity in lymphocytes. *Clin. Chim. Acta.* 256:197–201.

Canale, E. D., G. R. Campbell, J. J. Smolich, and J. H. Campbell. 1986. Cardiac Muscle. *In* Handbook of Microscopic Anatomy Vol. II. A. Oksche and L. Vollrath, editors. Springer-Verlag, New York. 8–51.

Chance, B. 1991. Optical Method. *Annu. Rev. Biophys. Biophys. Chem.* 20:1–28.

Chance, B., C. Barlow, J. Haselgrove, Y. Nakase, B. Quistorff, F. Matschinsky, and A. Mayevsky. 1978. Microheterogeneities of redox states of perfused and intact organs. *In* Microenvironments and Metabolic Compartmentation. P. A. Srere and E. W. Estabrook, editors. Academic Press, New York. 131–148.

Chance, B., and M. Lieberman. 1978. Intrinsic fluorescence emission from the cornea at low temperatures: evidence of mitochondrial signals and their differing redox states in epithelial and endothelial sides. *Exp. Eye Res.* 26:111–117.

Chance, B., B. Schoener, R. Oshino, F. Itshak, and Y. Nakase. 1979. Oxidation-reduction ratio studies of mitochondria in freeze-trapped samples. *J. Biol. Chem.* 254:4764–4771.

Demas, J. N., and G. A. Crosby. 1971. The measurement of photoluminescence quantum yields. *J. Phys. Chem.* 75:991–1024.

Denk, W., D. W. Piston, and W. W. Webb. 1995. Two-photon molecular excitation in laser-scanning microscopy. *In* Handbook of Biological Confocal Microscopy. J. B. Pawley, editor. Plenum Publishing, New York. 445–458.

Denk, W., J. H. Strickler, and W. W. Webb. 1990. Two-photon laser scanning fluorescence microscopy. *Science.* 248:73–76.

Dow, J. W., N. G. L. Harding, and T. Powell. 1981. Isolated cardiac myocytes. I. Preparation of adult myocytes and their homology with the intact tissue. *Cardiovasc. Res.* 15:483–514.

Eng, J., R. M. Lynch, and R. S. Balaban. 1989. Nicotinamide adenine dinucleotide fluorescence spectroscopy and imaging of isolated cardiac myocytes. *Biophys. J.* 55:621–630.

Estabrook, R. W. 1962. Fluorometric measurement of reduced pyridine nucleotide in cellular and subcellular particles. *Anal. Biochem.* 4:231–245.

Green, D. R., and J. C. Reed. 1998. Mitochondria and apoptosis. *Science.* 281:1309–1312.

Guezennec, C. Y., F. Lienhard, F. Louisy, G. Renault, M. H. Tusseau, and P. Portero. 1991. In situ NADH laser fluorometry during muscle contraction in humans. *Eur. J. Appl. Physiol.* 63:36–42.

Hall, C., and H. Kamin. 1975. The purification and some properties of electron transfer flavoprotein and general fatty acyl coenzyme a dehydrogenase from pig liver mitochondria. *J. Biol. Chem.* 250:3476–3486.

Hassinen, L., and B. Chance. 1968. Oxidation-reduction properties of the mitochondrial flavoprotein chain. *Biochem. Biophys. Res. Commun.* 31:895–900.

Kasischke, K. A., H. D. Vishwasrao, and W. W. Webb. 2001. Functional metabolic mapping using two-photon redox-fluorimetry reveals regional differences of energy flux within single neurons. *Biophys. J.* 80:431a. (Abstr.)

Kierdaszuk, B., H. Malak, I. Gryczynski, P. Callis, and J. R. Lakowicz. 1996. Fluorescence of reduced nicotinamides using one- and two-photon excitation. *Biophys. Chem.* 62:1–13.

Koenig, K., and H. Schneckenburger. 1994. Laser-induced autofluorescence for medical diagnosis. *J. Fluor.* 4:17–40.

Koke, J. R., W. Wylie, and M. Wills. 1981. Sensitivity of flavoprotein fluorescence to oxidative state in single isolated heart cells. *Cytobios.* 32:139–45.

Konig, K., P. T. So, W. W. Mantulin, B. J. Tromberg, and E. Gratton. 1996. Two-photon excited lifetime imaging of autofluorescence in cells during UVA and NIR photostress. *J. Microsc.* 183:197–204.

Kunz, W. S. 1986. Spectral properties of fluorescent flavoproteins of isolated rat liver mitochondria. *FEBS Lett.* 195:92–96.

Kunz, W. S. 1988. Evaluation of electron-transfer flavoprotein and a-lipoamide dehydrogenase redox states by two-channel fluorometry and its application to the investigation of b-oxidation. *Biochim. Biophys. Acta.* 932:8–16.

Kunz, W. S., and F. N. Gellerich. 1993. Quantification of the content of fluorescent flavoproteins in mitochondria from liver, kidney cortex, skeletal muscle, and brain. *Biochem. Med. Metabol. Biol.* 50:103–110.

Kunz, W. S., and W. Kunz. 1985. Contribution of different enzymes to flavoprotein fluorescence of isolated rat liver mitochondria. *Biochim. Biophys. Acta.* 841:237–246.

Kunz, W. S., A. V. Kuznetsov, K. Winkler, F. N. Gellerich, S. Neuhof, and H. W. Neumann. 1994. Measurement of fluorescence changes of NAD(P)H and of fluorescent flavoproteins in saponin-skinned human skeletal muscle fibers. *Anal. Biochem.* 216:322–327.

Kunz, D., C. Luley, K. Winkler, H. Lins, and W. S. Kunz. 1997. Flow cytometric detection of mitochondrial dysfunction in subpopulations of human mononuclear cells. *Anal. Biochem.* 246:218–224.

Kuznetsov, A. V., O. Mayboroda, D. Kunz, K. Winkler, W. Schubert, and W. S. Kunz. 1998. Functional imaging of mitochondria in saponin-permeabilized mice muscle fibers. *J. Cell Biol.* 140:1091–1099.

Maeda-Yorita, K., and K. Aki. 1984. Effect of nicotinamide adenine dinucleotide on the oxidation-reduction potentials of lipoamide dehydrogenase from pig heart. *J. Biochem. (Tokyo).* 96:683–690.

Masters, B. R. 1984. Noninvasive corneal redox fluorometry. *Curr. Top. Eye Res.* 4:139–200.

Masters, B. R., and B. Chance. 1993. Redox confocal imaging: intrinsic fluorescent probes of cellular metabolism. *In* Fluorescent and Luminescent Probes for Biological Activity. W. T. Mason, editor. Academic Press, New York. 44–57.

Masters, B. R., P. T. So, and E. Gratton. 1997. Multiphoton excitation fluorescence microscopy and spectroscopy of in vivo human skin. *Biophys. J.* 72:2405–2412.

Masters, B. R., P. T. So, and E. Gratton. 1998. Multiphoton excitation microscopy of in vivo human skin: functional and morphological optical biopsy based on three-dimensional imaging, lifetime measurements and fluorescence spectroscopy. *Ann. N.Y. Acad. Sci.* 838:58–67.

Nuutinen, E. M., J. K. Hiltunen, and I. E. Hassinen. 1981. The glutamate dehydrogenase system and the redox state of mitochondrial free nicotinamide dinucleotide in myocardium. *FEBS Lett.* 128:356–360.

Pacioretty, L. M., and R. F. J. Gilmour. 1998. Restoration of transient outward current by norepinephrine in cultured canine cardiac myocytes. *Am. J. Physiol.* 275:H1599–H1605.

Patel, M. S., N. N. Vettakkorumakankav, and T.-C. Liu. 1995. Dihydrolipoamide dehydrogenase: activity assays. *Methods Enzymol.* 252: 186–195.

Patterson, G. H., S. M. Knobel, P. Arkhammar, O. Thastrup, and D. W. Piston. 2000. Separation of the glucose-simulated cytoplasmic and mitochondrial NAD(P)H responses in pancreatic islet beta cells. *Proc. Natl. Acad. Sci. U.S.A.* 97:5203–5207.

Perham, R. N. 1991. Domains, motifs, and linkers in 2-oxo acid dehydrogenase multienzyme complexes: a paradigm in the design of a multifunctional protein. *Biochemistry.* 30:8501–8512.

Piston, D. W., S. M. Knobel, C. Postic, K. D. Shelton, and M. A. Magnuson. 1999. Adenovirus-mediated knockout of a conditional glucokinase gene in isolated pancreatic islets reveals an essential role for proximal metabolic coupling events in glucose-stimulated insulin secretion. *J. Biol. Chem.* 274:1000–1004.

Piston, D. W., B. R. Masters, and W. W. Webb. 1995. Three-dimensional resolved NAD(P)H cellular metabolic redox imaging of in situ cornea with two-photon excitation laser scanning microscopy. *J. Microsc. (Oxford).* 178:20–27.

Quistorff, B., J. C. Haselgrove, and B. Chance. 1985. High spatial resolution readout of 3-D metabolic organ structure: an automated, low-temperature redox ratio-scanning instrument. *Anal. Biochem.* 148: 389–400.

Romashko, D. N., E. Marban, and B. O'Rourke. 1998. Subcellular metabolic transients and mitochondrial redox waves in heart cells. *Proc. Natl. Acad. Sci. U.S.A.* 95:1618–1623.

Rumi, M., J. E. Ehrlich, A. A. Heikal, J. W. Perry, S. Barlow, Z. Hu, D. McCord-Maughon, T. C. Parker, H. Rockel, S. Thayumanavan, S. R. Marder, D. Beljonne, and J.-L. Bredas. 2000. Structure-property relationships for two-photon absorbing chromophores: bis-donor diphenylpolyene and bis(styryl)benzene derivatives. *J. Am. Chem. Soc.* 122: 9500–9510.

Saks, V. A., V. I. Veksler, A. V. Kuznetsov, L. Kay, P. Sikk, T. Tiivel, L. Tranqui, J. Olivares, K. Winkler, F. Wiedemann, and W. S. Kunz. 1998. Permeabilized cell and skinned fiber techniques in studies of mitochondrial function in vivo. *Mol. Cell. Biochem.* 184:81–100.

Schoffner, J. M. 1997. Oxidative phosphorylation defects and Alzheimer's disease. *Neurogenetics.* 1:13–19.

Scholz, R., R. G. Thurman, J. R. Williamson, B. Chance, and T. Bücher. 1969. Flavin and pyridine nucleotide oxidation-reduction changes in perfused rat liver. *J. Biol. Chem.* 244:2317–2324.

Segretain, D., A. Rambourg, and Y. Clermont. 1981. Three dimensional arrangement of mitochondria and endoplasmic reticulum in the heart muscle fiber of the rat. *Anat. Rec.* 200:139–151.

Shiino, A., M. Haida, B. Beauvoit, and B. Chance. 1999. Three-dimensional redox image of the normal gerbil brain. *Neuroscience.* 91:1581–1585.

Veeger, C., A. J. W. G. Visser, J. Krul, H. J. Grande, R. A. De Abren, and A. De Kok. 1976. Fluorescence studies on lipoamide dehydrogenase, pyruvate dehydrogenase complexes and transhydrogenase. *In* Flavins and Flavoproteins. T.P. Singer, editor. Elsevier, Amsterdam. 500–509.

Voltti, H., and I. E. Hassinen. 1978. Oxidation-reduction midpoint potentials of mitochondrial flavoproteins and their intramitochondrial localization. *J. Bioenerg. Biomem.* 10:45–58.

Wakebe, T., and E. van Keuren. 1999. The excitation spectra of two-photon induced fluorescence in xanthene dyes. *Jpn. J. Appl. Phys.* 38:3556–3561.

Wallace, D. C. 1999. Mitochondrial Diseases in Man and Mouse. *Science.* 283:1482–1493.

Williams, R. M., and W. W. Webb. 2000. Single granule pH cycling in antigen-induced mast cell secretion. *J. Cell Sci.* 113:3839–3850.

Xu, C., and W. W. Webb. 1996. Measurement of two-photon excitation cross sections of molecular fluorophores with data from 690 to 1050 nm. *J. Opt. Soc. Am. B.* 13:481–491.

Xu, C., and W. W. Webb. 1997. Multiphoton excitation of molecular fluorophores and nonlinear laser microscopy. *In* Topics in Fluorescence Spectroscopy, Vol. 5. J. R. Lakowics, editor. Plenum Press, New York. 471–540.

Xu, C., W. Zipfel, J. B. Shear, R. M. Williams, and W. W. Webb. 1996. Multiphoton fluorescence excitation: new spectral windows for biological nonlinear microscopy. *Proc. Natl. Acad. Sci. U.S.A.* 93: 10763–10768.